JOURNAL OF MATERIALS SCIENCE 19 (1984) 845–860

Surface softening in silicon by ion implantation

P. J. BURNETT, T. F. PAGE
Department of Metallurgy and Materials Science, University of Cambridge, Pembroke Street, Cambridge CB2 3QZ, UK

Load-variant microhardness tests have been used to investigate the hardness behaviour of ion-implanted (1 1 1) silicon wafers. A variety of ion doses, energies and species, including n-type, p-type and isovalent ions, have been implanted. At the high doses used (1 to 8 × 10^{17} ions cm^{-2}), all implantations resulted in a surface amorphous layer being formed. The microhardness behaviour has been interpreted in terms of the presence of a surface layer of lower hardness than the substrate. The thickness of this layer has been investigated experimentally using Rutherford backscattering and the results correlated with simple theoretical predictions. Finally, the microhardness behaviour of a soft layer on a harder substrate has been modelled in order to try to predict the hardness variations arising from differing layer thicknesses and different indentation sizes. It is concluded that the amorphous layer produced by implantation appears to show no variation of microhardness with load and has a hardness typically between 400 and 700 Vickers (VHN). Further, the previously reported "critical dose" of ~ 4 × 10^{17} ions cm^{-2} necessary to observe significant surface softening seems to correspond to the regime in which the amorphous layer shows a rapid increase with dose.

1. Introduction

Ion implantation has recently been looked to as a means of modifying the surface mechanical properties of a number of engineering components in order to lower friction, improve wear resistance and so extend working life (e.g. [1, 2]). Some success has been found in certain applications, notably those in which light adhesive wear processes play a major role in the degradation of the component (e.g. [1, 2]).

The present authors are investigating the effect of ion implantation on wear-related phenomena (e.g. indentation hardness behaviour, friction, surface plasticity, indentation fracture, phase transformations, etc.) for a range of materials. This paper presents the results of microhardness tests performed upon ion-implanted single-crystal (1 1 1) silicon. Previous work by Roberts and Page [3] has shown that implantations of N_2^+ ions above a "critical dose" of ~ 4 × 10^{17} ions cm^{-2} * into silicon and silicon carbide can result in both a reduction in indentation-induced lateral fracture and a marked surface-softening effect. Roberts and Page have suggested that this softening might principally be due to either (a) the formation of an amorphous layer,† (b) electronic interactions in the sub-amorphous material between moving dislocations and the donor or acceptor states introduced by implantation, or both.

In order to determine the effect of the thicknesses of implantation-induced amorphous layers, the present study has implanted silicon with a

*These implantations were carried out in the Pimento accelerator at AERE Harwell. This machine yields an unfiltered beam of ~ 75% N_2^+ at 90 keV, the balance being N^+ at 90 keV. The N_2^+ ions are assumed to split, on contact with the surface, into 2 × N^+ at 45 keV, thus the actual dose of N^+ will be 7/4 × the "stated dose" of N_2^+ (~ 16% of which is at 90 keV, the balance being at 45 keV).

†Silicon, in common with most group IV and III–V semiconductors, will become amorphous or microcrystalline under high-dose irradiation as, in these materials, self-annealing is slow: i.e. the disordering process predominates with respect to both the thermal and irradiation annealing processes during implantation [4].

0022–2461/84 $03.00 + .12

range of ion masses and energies. Further, the differing valence of the ions used has allowed any additional electronic effects of the dopant to be studied.

Simple theoretical estimates of the amorphous layer thicknesses have been carried out using existing damage distribution models and range data and the results compared with those experimentally determined using a channelled Rutherford backscattering (RBS) technique.

The variation of observed microhardness behaviour with decreasing indentation depth has been used in an attempt to estimate the hardness of the amorphous layer. Also, a simple model has been used to predict the hardness behaviour of a soft layer on a hard substrate, including the effect of changing both the layer thickness and the indentation size.

Besides exploring the effects of surface amorphous layers on microhardness behaviour, a further aim of this study has been to establish any possible significance of the "critical dose" for surface softening reported by Roberts and Page.

2. Amorphous layer thickness – theoretical determination

In order to estimate the extent of any amorphous layer produced by ion implantation into silicon, it is necessary to characterize the implantation in terms of the variations, with depth, of both implanted-species concentration and displacement damage. The concentration and damage profiles are usually assumed to be Gaussian in shape [4] and may be described in terms of the parameters R_P (mean projected range), ΔR_P (the standard deviation of R_P), $\langle X_D \rangle$ (the depth of the damage peak) and $\langle \Delta X_D \rangle$ (the standard deviation of $\langle X_D \rangle$).

The concentration profile parameters (R_P and ΔR_P) were determined using the Lindhard, Scharff and Schiøtt (LSS) model [5] as tabulated by Smith [6]. The relationship between range and damage distributions has been determined numerically by Winterbon, Sigmund and Sanders (WSS) [7] and their data have been used here to determine the damage parameters $\langle X_D \rangle$ and $\langle \Delta X_D \rangle$. The range and damage parameters for the ion–substrate–energy combinations considered here are shown in Table I, the energies being chosen to provide a reasonable variation in thickness of the amorphous layer produced.

The total number of displacements, $\nu(E)$, produced by one ion of energy E as it travels through the target, eventually coming to rest, may be estimated using the Kinchin–Pease model [8], as follows:

$$\nu(E) = \frac{E_c}{2E_d} \quad \text{for} \begin{cases} E \gg E_d \\ E > E_c \end{cases} \tag{1}$$

where E_d (the threshold displacement energy)* is the energy required to displace an atom of silicon from its structure site to create a Frenkel pair and E_c is the critical energy for efficient electronic excitation. At energies above E_c significant displacement damage ceases since the ions will preferentially lose energy by electronic excitation. When the energy drops below this value, electronic energy loss becomes less favourable and "hard sphere" collisions predominate (displacement damage). Both channelling and focused collision sequences may cause variations in $\nu(E)$ but, in this case, the effects were assumed negligible and, for channelling at least, this was confirmed by the absence of channelling tails on the RBS depth profiles. To a reasonable approximation [10]:

TABLE I (1 1 1) silicon range and damage parameters

Species	Energy (keV)	Range parameters (μm)		Damage parameters (μm)	
		R_P	ΔR_P	$\langle X_D \rangle$	$\langle \Delta X_D \rangle$
N	45	0.136	0.0472	0.110	0.0402
N	90	0.275	0.077	0.222	0.0656
Al	300	0.472	0.115	0.372	0.107
As	350	0.217	0.0672	0.179	0.091
Si	120	0.172	0.055	0.137	0.049
Si	300	0.442	0.112	0.352	0.100
N	100	0.300	0.078	0.375	0.067
N	220	0.600	0.110	0.480	0.094
N	400	1.000	0.140	0.800	0.120

*Generally, in a crystalline material, the displacement energy is multi-valued, displaying a crystallographic anisotropy. However, for our purposes a single value of 12.9 eV [9] was assumed.

$$E_c \text{ (in keV)} \simeq A \qquad (2)$$

where A is the ingoing ion mass in a.m.u.

Since the dose is known, and assuming all the ions remain in the target, the total number of displacements may be calculated as:

$$\text{Total displacements (per cm}^2\text{)} = \nu(E) \times \text{dose (ions cm}^{-2}\text{)}. \qquad (3)$$

Hence the Gaussian damage profile may be given as (e.g. [11]):

$$\text{Displacements per cm}^3 = \frac{\nu(E) \times \text{dose}}{\langle \Delta X_D \rangle (2\pi)^{1/2} \times 10^{-4}} \exp\left[\frac{-\frac{1}{2}(X - \langle X_D \rangle)^2}{\langle \Delta X_D \rangle^2}\right] \qquad (4a)$$

where $\langle X_D \rangle$ and $\langle \Delta X_D \rangle$ are the damage parameters in micrometres and X is the depth below the original surface (also in micrometres). No allowance was made for either sputtering or surface expansion. Equation 4a may be rewritten in terms of displacements suffered per substrate atom by simply dividing by the atomic density of the target, ρ_A, (in atoms cm^{-3}) to give:

$$\text{Displacements per atom (DPA)} = \frac{\nu(E) \times \text{dose}}{\langle \Delta X_D \rangle (2\pi)^{1/2} \times 10^{-4}} \frac{1}{\rho_A} \exp\left[\frac{\frac{1}{2}(X - \langle X_D \rangle)^2}{\langle \Delta X_D \rangle^2}\right]. \qquad (4b)$$

Similar expressions for the Gaussian composition profile may be obtained from Equation 4a by replacing the damage parameters, $\langle X_D \rangle$ and $\langle \Delta X_D \rangle$, with the range parameters, R_P and ΔR_P, and by taking $\nu(E)$ as unity (e.g. [11]). The relative positions of the concentration and damage profiles are shown schematically in Fig. 1, from which it can be seen that the peak of the damage distribution lies closer to the surface than that of the concentration profile.

By applying an amorphization criterion such as that proposed by Cristel *et al.* [12], in which amorphization is assumed to occur wherever a critical damage level is exceeded, it is possible to evaluate the thickness and position of any amorphous layer produced by implantation. For silicon, a value of 0.1 DPA was experimentally determined by Cristel *et al.* and this value was used here. Fig. 2 demonstrates how the size and position of the amorphous layer varies with increasing ion dose at constant ion energy. The Gaussian distribution calculated

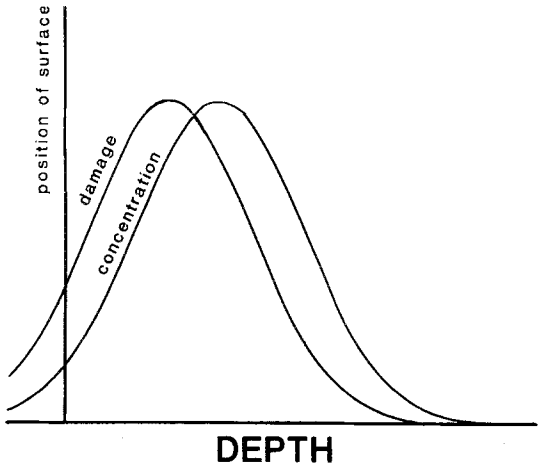

Figure 1 A schematic representation of the depth profile of the concentration of the implanted species after implantation with a monoenergetic beam of ions. Also shown is the displacement damage-depth profile resulting from the implantation. The relative positions of the concentration and damage curves should be noted (i.e. the implantation peak is always deeper than the damage peak), as should the non-zero values of both profiles at the surface.

from Equation 4b simply increases in amplitude with increasing dose and results in an increasing displacement level at the surface but with the maximum damage $\langle X_D \rangle$ below the surface. At low doses, no part of the damage profile exceeds the amorphization criterion and no amorphous material results (Fig. 2a). When the dose is increased, an amorphous region is produced as a subsurface zone enclosed between the crystalline substrate and a damaged, but still, crystalline surface layer (Fig. 2b). Further increase in the dose results in this layer expanding until, when the DPA at the surface itself exceeds the amorphization criterion, the amorphous layer extends inwards from the surface (Fig. 2c). Once this latter stage is passed, the rate of increase of amorphous layer thickness with dose approximately halves, since it is now principally controlled by the extension of only one half of the Gaussian curve into the subsurface material (Fig. 2d).

Fig. 3 shows the predicted variation of thickness of the amorphous zone/layer with dose for the various ion species used in this study. For each curve, the intercept on the dose axis corresponds to the peak of the damage distribution just reaching the amorphization criterion, while the point at which the slopes show a discontinuity (▲) corresponds to the amorphous layer just reaching the

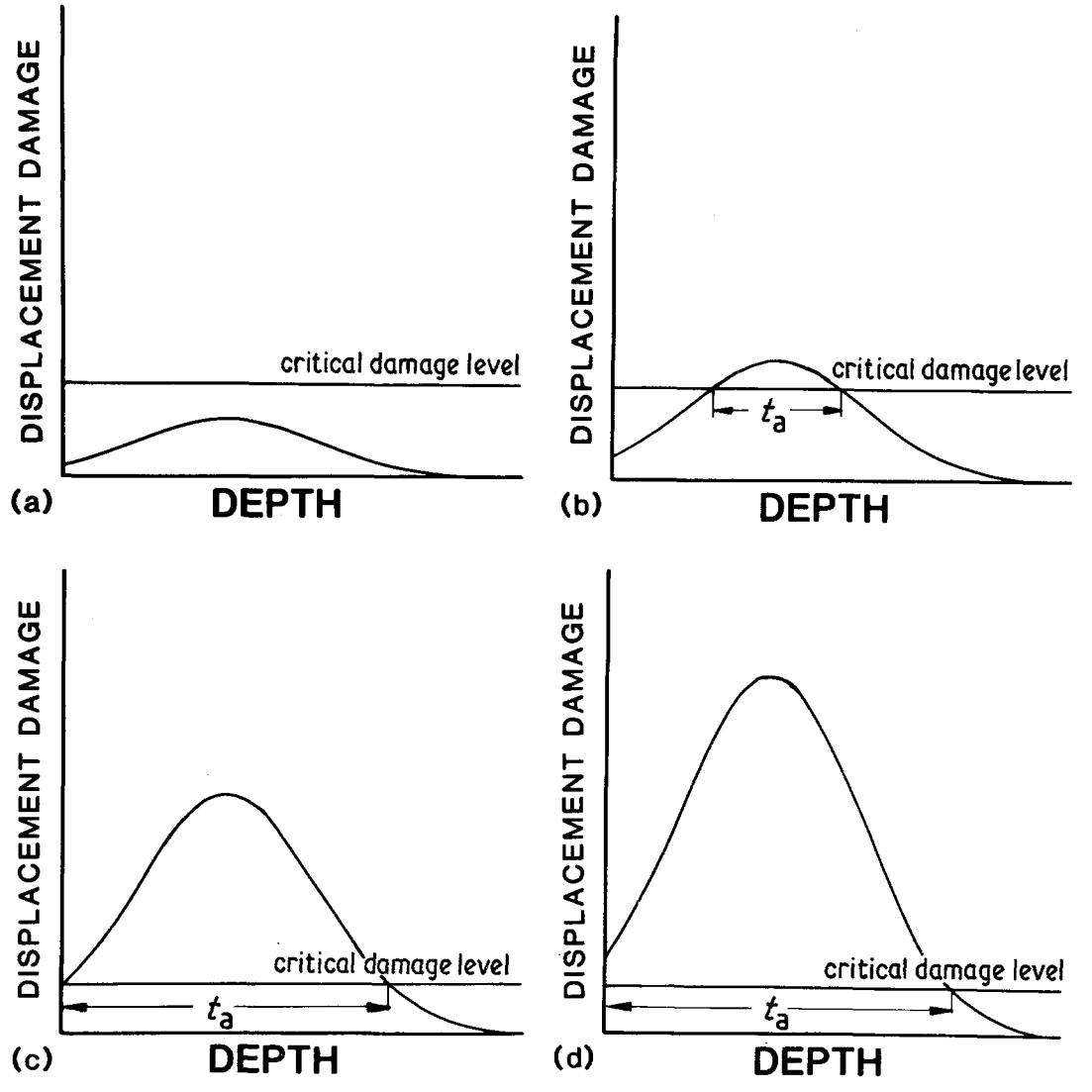

Figure 2 Schematic representations of the variation of the amorphous-layer thickness, t_a, with the amplitude of the displacement damage: depth profile at relative doses of 1, 2, 8 and 12. (a) No amorphous layer is produced, as the peak of the damage distribution lies below the critical damage level for amorphization; (b) the formation of a subsurface amorphous zone as the dose (and hence damage level) is increased; (c) the formation of a surface amorphous layer as the displacement level at the surface reaches the critical value; (d) further growth of the amorphous layer into the substrate only as the damage level is increased beyond that of (c). For convenience the scale of the damage axis has been reduced in (c) and (d).

surface (Fig. 2c). Beyond this point, the rate of increase of layer thickness with dose decreases. It may be seen that all specimens tested here exceed this dose for surface amorphization (see Table II for doses).

3. Specimen preparation

Semiconductor-grade silicon supplied as wafers of off-[1 1 1] sheet normal (courtesy of Texas Instruments) were used for all implantations. The doping levels (where known) of these wafers are given in Table II. The wafers were supplied pre-polished and no further surface treatments were performed prior to implantation.

The implantations were performed at AERE Harwell using the Cockcroft–Walton 500 kV implantation facility and the Pimento prototype implantation machine (e.g. [1]). The Pimento has a large specimen area, enabling whole wafers to be implanted. Specimens for implantation in the

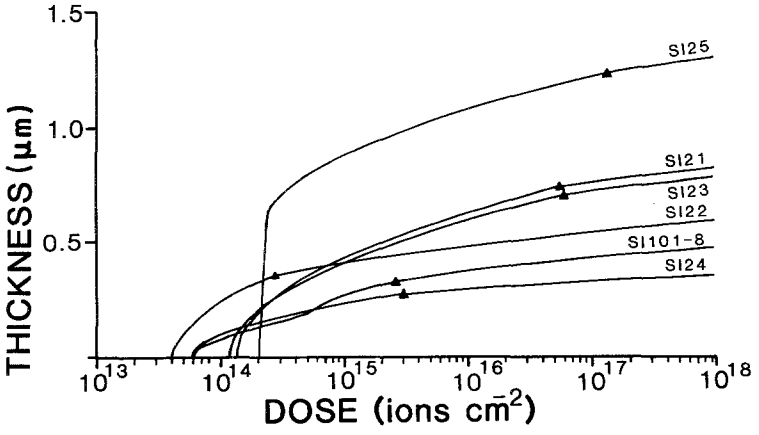

Figure 3 The predicted variation of amorphous layer thickness with dose for the various ion:energy combinations used in this study. The annotations correspond to the ion:energy combinations given in Table II. Note that SI25 and SI101–8 are all multiple implants and that, for the former, the dose axis corresponds to the level of the 100 keV implant while, for the latter, the "stated dose" is as defined in Section 1. The relative doses for SI25 were chosen to ensure that a large amorphous layer was rapidly established. The relative doses of N_2^+ and N^+ in the Pimento beam result in a kink occurring in the dose:thickness curve as the damage associated with the lower dose, higher energy component (N^+ at 90 keV) becomes important. On each curve, ▲ marks the dose at which the amorphous layer just extends to the surface, as in Fig. 2c. Thus for all doses between such points and the intercept of each curve with the dose axis (the onset of amorphization), a subsurface amorphous zone is expected (Fig. 2b). Beyond these points the amorphous layer is thickening by extension into the substrate only (Fig. 2d).

Cockcroft–Walton facility were cleaved to size (~ 30 mm diameter) along the ⟨1 1 0⟩ directions after scoring with a diamond stylus. Details of the implantations may be found in Table II. "Standard" implantation conditions were used throughout (e.g. current densities of ~ 3 to 4 μA cm^{-2} giving rise to temperature rises of ~ 250° C on the specimen). Other than mounting the sample orthogonally to the beam, no special precautions were taken to ensure that channelling of the beam did not occur. Despite the background chamber vacuum being typically of the order of ~ 10^{-5} to 10^{-7} torr, significant levels of carbon, and other contaminants, were not revealed by subsequent RBS analysis.

TABLE II Implantation doses and energies; resulting amorphous layer thicknesses

Specimen	Species	Initial bulk substrate doping (atoms cm^{-3})	Nominal dose (ions cm^{-2})	Energy (keV)	Implanter†	Amorphous layer thickness	
						Predicted‡ (μm)	Observed (RBS) (μm)
SU101	–	–	–	–	–	–	–
SI101	N_2^+	9.4×10^{13} Sb	1×10^{17}	90	Pimento	0.43	0.46
SI102	N_2^+	9.4×10^{13} Sb	2×10^{17}	90	Pimento	0.45	0.47
SI104	N_2^+	9.4×10^{13} Sb	4×10^{17}	90	Pimento	0.46	0.50
SI106	N_2^+	9.4×10^{13} Sb	6×10^{17}	90	Pimento	0.467	0.72
SI108	N_2^+	9.4×10^{13} Sb	8×10^{17}	90	Pimento	0.47	0.73
SI21	Al^+	5.9×10^{14} Sb	5×10^{17}	300	C–W	0.82	~ 0.8–0.9§
SI22	As^+	1.8×10^{15} B	5×10^{17}	350	C–W	0.58	0.60
SI23	Si^+	unknown	5×10^{17}	300	C–W	0.76	unresolvable§
SI24	Si^+	unknown	4×10^{17}	120	C–W	0.34	~ 0.48§
SI25	N^+	unknown	1.5×10^{17}	100			
			2.0×10^{17}	220	C–W	1.22	1.05
			2.5×10^{17}	400			

†C–W = Cockcroft–Walton implantation facility.
‡From the model of Section 2.
§ Uncertainty arises from superposition of the damage and implant peaks for species close to silicon in atomic number.

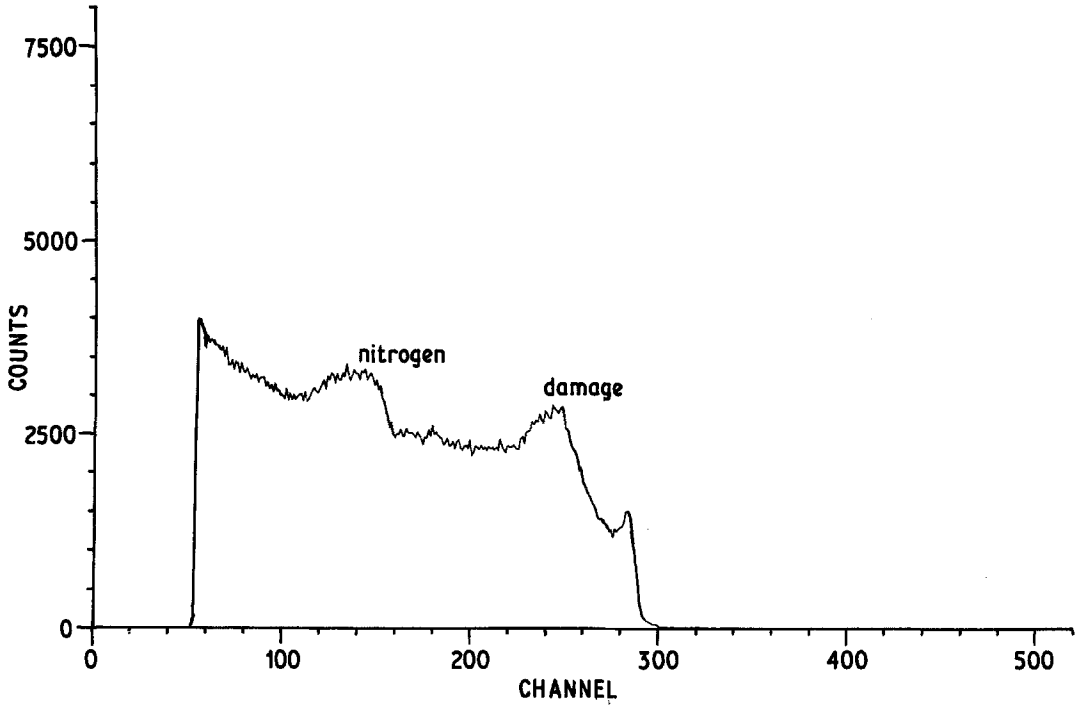

Figure 4 A channelled ⟨1 1 1⟩ Rutherford backscattering spectrum for specimen SI108 (8×10^{17} N_2^+ ions cm^{-2}) showing clearly the scattering peaks corresponding to the implanted species and the damaged (amorphous) surface. (Spectrum recorded at 4 keV per channel.)

4. Amorphous layer thickness — experimental determination

A channelled Rutherford backscattering technique was adopted as a means of determining both the depth of penetration of the ions and the extent of the damaged layer produced. The analysis was carried out in the IBIS (intense bunched ion source) accelerator at AERE Harwell using 2 MeV He^+ ions throughout with a solid-state detector mounted at an angle of 160° to the incident beam. In all cases, the ⟨1 1 1⟩ channelling direction close to (within 2 to 3° of) the surface normal was utilized. The specimens analysed were those previously used for microhardness testing (see Section 5). A typical spectrum of scattered ion energies is shown in Fig. 4. In order to convert the energy spectra to depth spectra a number of simplifying assumptions were made: (a) that the electronic stopping power of the ions by the substrate remains constant as the ion travels (and slows down) into the target; (b) that the electronic stopping power of the ion by the substrate after scattering remains constant until the ion leaves the substrate (although this value is different from that of (a) since the ion has lost energy by scattering); (c) that the stopping power of the implanted layer is identical to that of the unimplanted substrate (i.e. no account is taken of density and composition changes produced by the implantation). The stopping powers used are those tabulated by Ziegler [13] and, using these, the subsurface thicknesses of the amorphous layers were calculated from the measured size of the damage peak using the treatment given by Carter and Grant [4].

Table II lists the experimentally determined amorphous-layer thicknesses together with those calculated using the model of Section 2. From these results it may be seen that the depths for the lower-dose specimens (e.g. SI101, SI21) correspond fairly well with the calculated depths, but that the high-dose nitrogen implantations (SI106 and SI108) both produce a damaged layer that is much thicker than predicted. As will be seen later, this is an important effect and may be a result of: (a) structural alteration of the surface as the implantation proceeds, resulting in a more ion-transparent layer, (b) surface stresses, (c) channelling or (d) recoil implantation.

Both transmission and scanning electron microscopy methods (TEM and SEM) were also

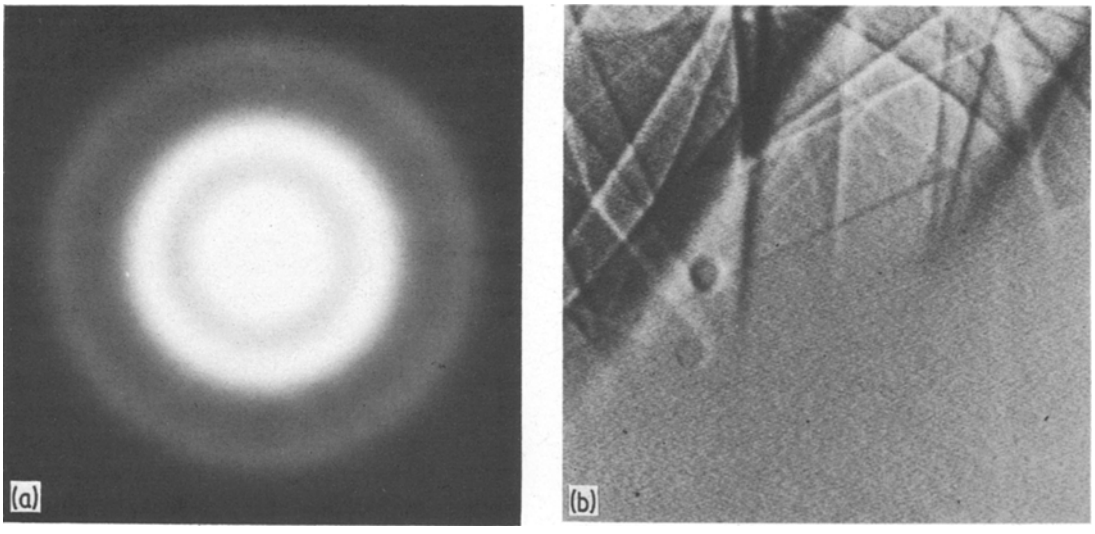

Figure 5 (a) A selected area electron diffraction pattern (100 kV) of part of the implanted surface of SI108 (8×10^{17} N_2^+ ions cm^{-2}). Only diffuse diffraction rings are present, indicating that the specimen is amorphous. The specimen was prepared by ion-beam thinning from the unimplanted side of a 3 mm disc cut from the implanted wafer. (b) A wide-area electron-channeling pattern (backscattered electron mode: 30 kV) of SI25 (N^+-implanted silicon), taken with the scanned area crossing the implanted–unimplanted boundary. The implanted region shows no channelling contrast, indicating that the surface is amorphous to at least a depth of ~ 100 nm (see text).

used to investigate the amorphicity of the specimens – see Fig. 5. In TEM, electron diffraction was employed on specimens carefully "back-thinned" towards the implanted surface (Fig. 5a) while, in SEM, the disappearance of electron channelling on crossing boundaries between unimplanted and implanted material was looked for as confirmation that the amorphous layer extended to the surface (Fig. 5b). On this latter point, Joy *et al.* [14] cite channelling contrast as arising from the topmost ~ 100 nm of a bulk silicon sample (at 20 to 30 keV electron beam voltage), which nicely correlates with the expected scale of any intermediate crystalline layer between the surface and the amorphous zone. Indeed, other work [15, 16] has confirmed that degraded channelling patterns can still be obtained in cases where such a damaged but crystalline surface layer is still present.

5. Microhardness testing – method and results

Microhardness indentations were made and measured using a Leitz Miniload under constant lighting conditions in a darkened room. Five indentations at each load of 10,* 25, 50, 100, 200, 300, 500 and 1000 gf were made on each specimen, these indentations corresponding to indenter penetration depths of typically ~ 0.7 to 7 μm. Each testing session consisted of at least two, usually three, specimens being tested consecutively so as to minimize the effect of variation of operator performance. Each specimen was tested at least twice. A standard loading-cycle time of 25 sec was used for all tests to eliminate variation in hardness due to indentation creep. For all tests, a Vickers profile diamond indenter was used. In order to remove the effects of hardness anisotropy (e.g. [18]) the indenter was always oriented with its diagonals parallel to orthogonal $\langle 1\,\bar{1}\,0\rangle$ and $\langle 1\,1\,\bar{2}\rangle$ traces of the $\{1\,1\,\bar{1}\}$ and $\{1\,\bar{1}\,0\}$ cleavage planes. The hardness at each load was calculated from the mean of ten diagonals measured. In addition, the dependence of observed hardness on load and thus indentation size (the indentation size effect, ISE) was also measured for unimplanted silicon. The means adopted here of quantifying the ISE was by a Meyer approach [3, 19], whereby an ISE index, m, is defined by

$$L = ad^m \tag{5}$$

*In the high-dose N_2^+ specimen (SI108), the 10 gf indentations could not be seen owing to poor contrast from the implantation-roughened surface (e.g. [17]).

where L is the load, d is the indentation diagonal and a is a constant. Hence for $m < 2$ the observed hardness increases as the applied load decreases; for $m = 2$ hardness is constant with load, while for $m > 2$, the observed hardness decreases with decreasing load. Not only do the parameters a and m describe the ISE behaviour of a solid but they also allow effective hardness values at any given contact size to be estimated.

The general trend was for the low-load hardness of the implanted material to be less than that for the unimplanted material, the hardnesses converging at the higher loads (e.g. see Fig. 11). The absolute values of measured hardness were found to vary slightly between sessions for any given specimen, but the trends exhibited were similar.

Since unimplanted silicon exhibits a strong indentation size effect with an ISE index of ~ 1.7, the presence of a thin ($\lesssim 0.5\,\mu$m) softer layer at the surface is expected to modify the ISE behaviour such that the specimen shows a lesser increase of hardness as the load is decreased. Eventually specimens with larger amorphous layers may show an absolute softening.

Since the low-load microhardness behaviour is the more sensitive to a soft surface layer, the 25 gf and 50 gf hardnesses were plotted against the experimental amorphous layer thicknesses obtained by varying the dose of N_2^+ into silicon (specimens SI101–8) and this is shown in Fig. 6. Unfortunately, the indentation sizes of loads of 10 gf could not be measured sufficiently reproducibly for any significant variations in very-low-load hardness behaviour to be seen and these data have not been included. Fig. 7 is a similar plot of hardness against the varying amorphous layer thicknesses further obtained by variation of dose, energy and species, i.e. this would show any effects due to varying the valency of the implanted species. From both figures it may be seen that the microhardness values measured at 25 gf and 50 gf decrease with increasing amorphous-layer thickness and converge to similar values when the layer thickness is $\gtrsim 0.8\,\mu$m. These results imply not only that the amorphous layer is softer than the substrate but also that the layer itself shows little (if any) variation of identation hardness with load, at least at two low loads used here (i.e. the layer appears to have an ISE index of ~ 2). These are not unreasonable deductions since the yield stress of the defect-rich open structure of the amorphous layer might be expected to be lower than that of the crystalline parent. Further, plastic deformation of the amorphous material almost certainly occurs by micromechanisms differing from the parent (e.g. densification [18], shear band propagation [20, 21], etc.). The detailed origins of the ISE effect in solids is still unclear (e.g. [19, 22]) but are thought to be concerned with elastic recovery (i.e. residual stresses around the indentation), surface effects (e.g. the effects of chemisorbed layers) and, particularly, both the absolute and relative scales of the indentation and the materials' microstructure (i.e. true

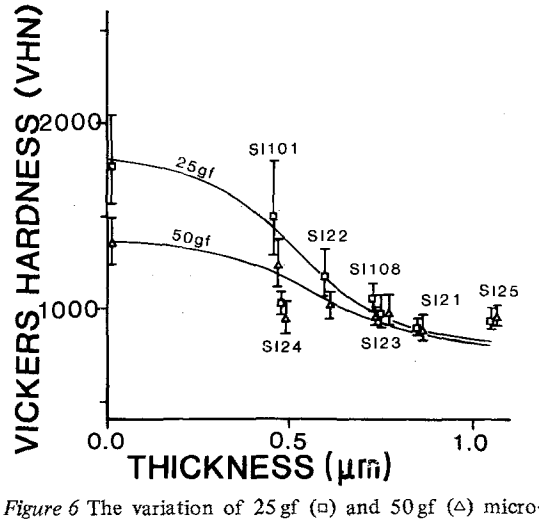

Figure 6 The variation of 25 gf (□) and 50 gf (△) microhardness with experimentally determined amorphous layer thickness for silicon implanted with N_2^+ at varying doses (see Table II). The error bars are 2σ.

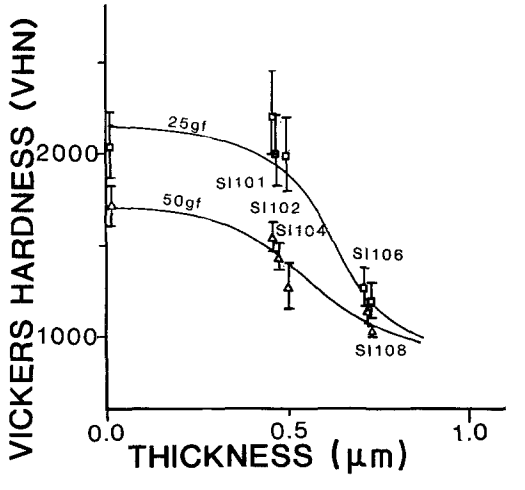

Figure 7 The variation of 25 gf (□) and 50 gf (△) microhardness with experimentally determined amorphous layer thickness for silicon implanted with varying ion–dose–energy combinations (see Table II). The error bars are 2σ.

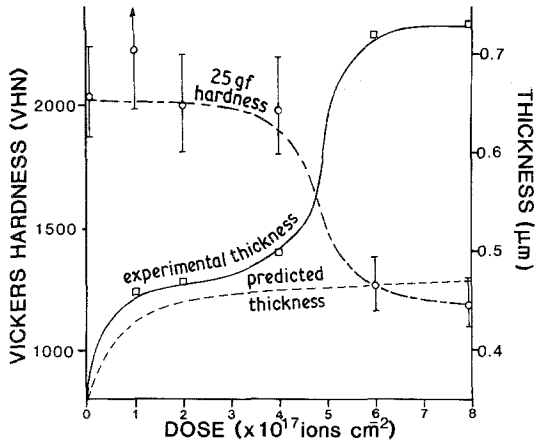

Figure 8 The variation of 25 gf hardness, experimental and predicted amorphous layer thicknesses with dose of N_2^+ in silicon. Note the correspondence between the rapid fall in 25 gf hardness and the rapid increase in the experimental amorphous layer thickness. The error bars for the 25 gf hardness are 2σ.

activation volume effects for deformation coupled with slip impedance by obstacles in the microstructure). Thus an ISE of ~ 2 (i.e. hardness independent of load) is not unreasonable for a highly defective, structureless layer of low yield stress.

The valence of the implanted species appears not to play a major role in the observed surface softening effect since none of the species used, whatever their valence (i.e. p-type (As, N), n-type (Al) or isovalent (Si)), produced effects other than being consistent with the trends observed in Fig. 6 for silicon implanted with N_2^+ ions.

From Figs. 6 and 7 it can be seen that the observed hardness at small indentation sizes decreases rapidly once the indentation can be substantially contained within the surface amorphous layer. Thus, there might be expected to be a "critical dose" to produce an apparent softening and this dose should vary with the size (i.e. depth) of the indentations used. However, as was seen in the previous section, the *predicted* amorphous-layer thickness increases only slowly with dose as shown in Figs. 3 and 8. Also, in the previous section, it was shown that the *observed* amorphous-layer thickness (in silicon at least) shows an unexpected rapid increase at a dose of ~ 4×10^{17} to 6×10^{17} N_2^+ cm^{-2}. This is also plotted in Fig. 8, as is the 25 gf indentation hardness as a function of dose. The rapid change in 25 gf indentation hardness may be seen to correspond to this unpredicted rapid increase in amorphous layer thickness.

Thus, while the amorphous layer should be increasing only gradually with dose, this effect, whatever its origins, rapidly increases the layer thickness to that where it markedly affects hardness measurements made at ~ 1 μm indentation depth.

Almost certainly, the rapid change of layer thickness with dose in the 4×10^{17} to 6×10^{17} N_2^+ cm^{-2} range largely accounts for the "critical dose" effect previously reported by Roberts and Page [3] as being necessary to produce significant softening as revealed by the hardness behaviour standardized to a 10 μm indentation diagonal ($H_{10\,\mu m}$), and would probably reveal itself as a discontinuous change in other near-surface properties also.

6. Surface softening – an empirical model

Given the results of the foregoing sections, it seemed worthwhile to attempt to model the hardness behaviour expected of a composite specimen having a soft layer over a hard substrate. In this way, the systematic variations of the hardness with both the size of the indentation and the layer thickness were explored and will now be presented.

The modelling of the hardness behaviour of a material possessing a surface layer, hard or soft, is a complex problem. Some attempts have been made to establish theoretical models for the load–hardness (penetration) behaviour of materials with "thin" surface coatings (e.g. [23]). However, these models are complex and usually deal with indentation by spheres or cones at relatively large loads (and hence large penetrations) for relatively macroscopic coatings (e.g. in [23] coatings up to 2 mm thick are considered). There seems no model simply applicable to the case considered here of a very thin coating on a substrate displaying marked ISE behaviour.

Consequently, owing to a lack of theoretical understanding of the stress–displacement distribution around an indentation penetrating a thin (< 1 μm) soft coating on a stiff substrate, let alone the additional ISE effects, an empirical approach was adopted for this study.

Sargent [24] proposed a simple law of mixtures approach whereby

$$H_{\text{effective}} = \frac{H_1 V_1 + H_2 V_2}{V_1 + V_2} \qquad (6)$$

where $H_{\text{effective}}$ is the resultant hardness, H_1 and H_2 are substrate and surface-layer hardness values, respectively, and V_1 and V_2 are the deforming volumes of the substrate and layer, i.e. the respec-

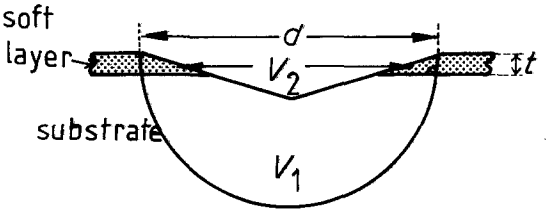

Figure 9 The deformation geometry assumed for calculating the effective hardness of a soft layer on a hard substrate. Volumes V_1 and V_2 are the "substrate" and "layer" portions, respectively, on a hemispherical cap of diameter d, where d is the indentation diagonal of a hardness impression made by a Vickers profile indenter and t is the surface-layer thickness.

tive volumes controlling the measured hardness for a given geometry of deformation. The spherical-cavity model of the indentation process (e.g. [25, 26]), whereby displaced material is accommodated by radially directed elastic compression, is the usual model used for brittle materials (e.g. [18]) and suggests that the geometry of Fig. 9 would be a simple starting point; i.e. it is assumed that the only material affecting hardness is contained in a hemispherical cap of diameter equal to the diagonal of a Vickers indentation. For a Knoop indenter, an ellipsoidal section would be more appropriate. It is further assumed that the indenter will penetrate the surface layer (this has been observed with Knoop indentations on ion-implanted sapphire [15]) though, in reality, the softer layer may be extruded from between the substrate and the indenter (see Fig. 10) to produce pile-up. Since this pile-up probably contributes little to the support of the load it is ignored in the calculations which follow.

In the first instance, Equation 6 assumes that H_1 and H_2 are constants. However, as V_1 and V_2 change, the ISE behaviour of the H values might also be expected to be reflected in the final value of $H_{\text{effective}}$. For example, if H_1 displayed a large ISE with its value rising rapidly as V_1 diminishes, then its effect will be to cause $H_{\text{effective}}$ to rise before falling to the values predicted by the simple law of mixtures expression (that is with H_1, H_2 assumed constant). The results of the previous section indicate that the silicon substrate displays strong ISE behaviour although the amorphous layer apparently does not. Thus, in this case, it is only necessary to incorporate the ISE behaviour of the substrate into Equation 6 by combining Equation 5 (which describes the ISE) with the definition of indentation hardness

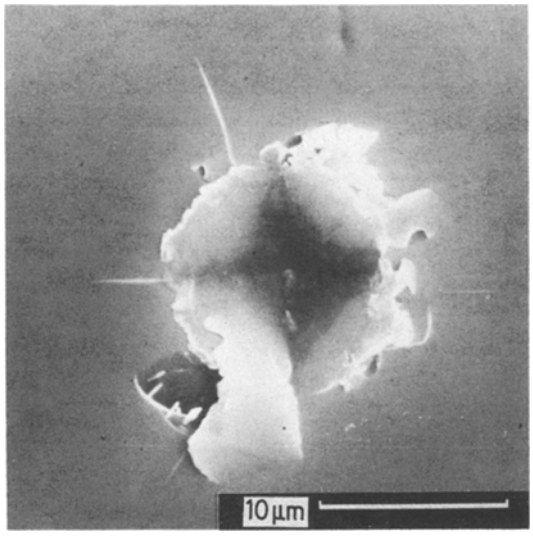

Figure 10 A scanning electron micrograph (secondary electron model) of a 100 gf hardness impression made in silicon implanted with 5×10^{17} Al^+ ions cm^{-2} (SI121). The barrelled shape of the impression is probably due to plastic pile-up [e.g. 27]. "Extrusion" of the softer surface layer during indentation is apparent.

$$H = \frac{bL}{d^2} \tag{7}$$

to produce

$$H_1 = cd^{m-2} \tag{8}$$

where b and c are constants.

Without this correction, Equation 6 simply predicts a decrease in hardness with decreasing indentation size (i.e. as the softer layer starts to assume dominance). However, with the correction of Equation 8 incorporated, a more complex variation of $H_{\text{effective}}$ with indentation diagonal is predicted which now shows the experimentally observed effect (Fig. 11) of H rising slightly before the decrease at small indentation sizes. An even better fit was found by the further incorporation of an empirical factor $V_1/(V_1 + V_2)$ into the H_1 term in Equation 6, i.e.

$$H_1 V_1 = cd^{m-2} \frac{V_1^2}{V_1 + V_2}. \tag{9}$$

This weights the importance of the substrate hardness according to the relative deformation volumes – i.e. it weights $H_{\text{effective}}$ in favour of the hardness of the near-surface material at low loads. Thus, when $V_1 \gg V_2$ the factor is ~ 1, while for $V_2 \gg V_1$ the factor is ~ 0 and the value of H_1 is unimportant (as is its ISE behaviour). Fig. 11

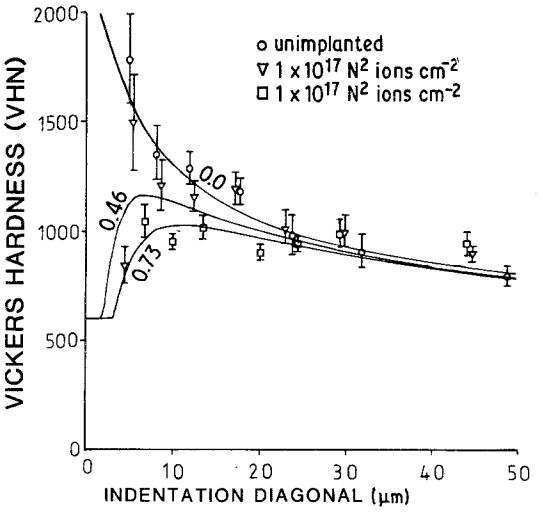

Figure 11 Data points showing the experimentally determined hardness: indentation diagonal behaviour for unimplanted silicon and for silicon implanted with 1×10^{17} and 8×10^{17} N_2^+ ions cm^{-2} (specimens SI101 and SI108 respectively). Also plotted are the computed curves (using the treatment of Section 6) for the hardness behaviour of silicon possessing surface layers of 0.0, 0.46 and 0.73 μm thickness with a layer hardness of 600 VHN and ISE index of 2.0. The error bars are 2σ.

shows the correlation between this model and the experimentally observed behaviour.

A further complication is that of differing amounts of elastic recovery occurring in the substrate and layer volumes. Elastic recovery should always reduce the unloaded measured diagonals of hardness impressions by a factor (elastic strain) of $\sim H/E$ (e.g. [27]). While it is anticipated that $H_{\text{effective}}$ will be predominantly affected by recovery in the surface layer rather than the substrate, a range of complex effects might be expected, owing to the constraint which recovery strains in the bulk of the sample might impose on the surface layer. However, the effects will be small, and, in the absence of any proven analytical approach, were not considered further. It should also be noted that the present case of a soft surface-layer implies less elastic recovery in the surface after implantation, resulting in a further slight reduction in observed hardness. For the purposes of computation, two simplifying assumptions about the nature of the amorphous layer were made, namely: (a) that all amorphous layers produced by ion bombardment into silicon have roughly the same hardness and (b) that the hardness of this layer is in the range 400 to 700 VHN which was experimentally estimated by extrapolation of the behaviour shown in Figs. 6 and 7.*

Using Equation 6 modified by Equation 9, the hardness behaviour of a composite specimen was computed as a function of both indentation size and soft-layer thickness. Fig. 12 shows typical results evaluated for a layer hardness of 600 VHN (with no ISE) and a substrate characterised by $H_{10\,\mu m} = 1325$ VHN and $m = 1.7$ (i.e. the values experimentally determined for unimplanted silicon). In Fig. 12a, the variation of indentation hardness with both indentation size and layer thickness is shown. Fig. 12b is a contour map of Fig. 12a. Important trends shown by these diagrams are:

1. a plateau of near-constant hardness for large indentation sizes (typically $> 35\,\mu$m) where the behaviour of the substrate dominates;

2. for zero layer thickness, the rear face of the diagram shows the ISE behaviour of silicon with hardness rising rapidly at small indentation sizes;

3. for intermediate layer thicknesses ($0 \rightarrow 1.5\,\mu$m) and decreasing indentation diagonals, there is a noticeable rise in hardness before the softer surface layer dominates and, on the diagram, this is seen as a ridge extending away from the rear hardness peak for unimplanted silicon;

4. for large layer thicknesses ($> 1.5\,\mu$m) the ridge is negligible and the hardness falls gently with decreasing indentation size until H_2 is reached. The low hardness plateau at the right of the diagram corresponds to the indentation being wholly contained in the soft layer.

Three hardness–indentation-diagonal sections are shown boldly in Fig. 12a with corresponding traces shown in Fig. 12b. These correspond to the amorphous-layer thicknesses of specimens SI101 and SI108 together with an unimplanted specimen. These three curves are those already shown in Fig. 11, where an encouraging fit to the experimentally observed behaviour was found.

7. Discussion

The results presented in the previous sections rely upon the correlation of a number of exper-

*An alternative estimate can be made by assuming that the difference between the 1 kg hardness of silicon (~ 900 VHN) and the amorphous layer hardness is similar in magnitude to that observed in other covalent materials which may exist in amorphous and crystalline states: e.g. silica, for which the Mohs hardness of quartz is 7.0 and that of glassy silica only 4.9 [28].

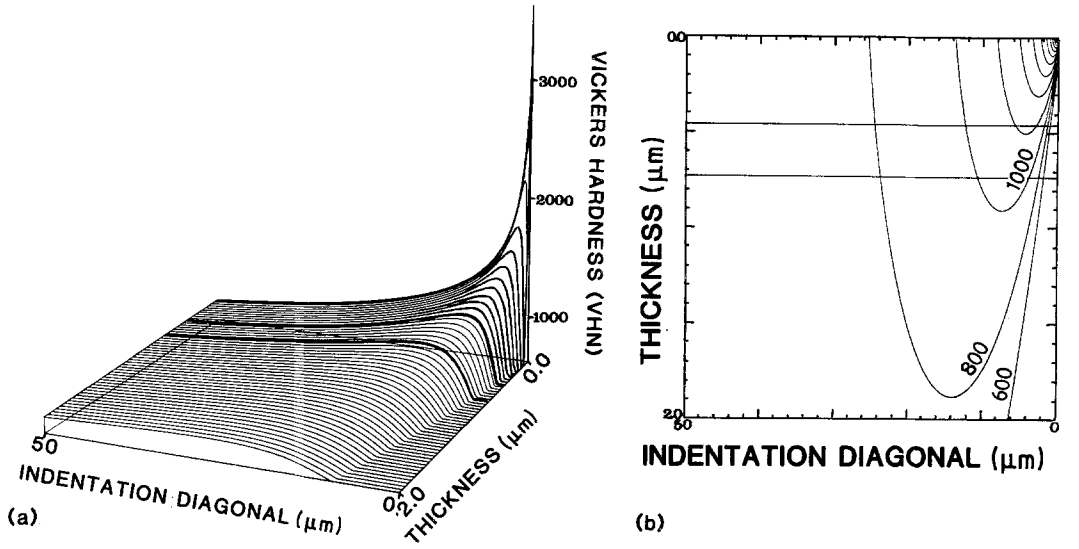

Figure 12 (a) A three-dimensional representation of hardness as a function of indentation diagonal and surface-layer thickness for a substrate of silicon (ISE index = 1.7, $H_{10\,\mu m}$ = 1325 VHN) with a surface layer of hardness 600 VHN and an ISE index of 2.0. The curves indicated in bold correspond to those shown in Fig. 11. (b) A contour map of (a); the traces of bold curves of (a) are also marked.

imental methods and calculations; this raises a number of points for further discussion.

First, the interesting changes in hardness behaviour are observed to occur, as expected, at small (~ 4 to 20 μm) indentation diameters. Invariably, in the making and measurement of such small indentations, there are always errors associated with the operator, the specimen or the measuring system. Despite attempts at minimizing the effects of operator error during the microhardness testing (e.g. maintaining constant lighting conditions), some variations in results from session to session did occur. These may not necessarily be due purely to operator error, or limitations of the optics, since it is possible that the specimens may not have been evenly implanted. This is particularly true for implantations performed on the Pimento machine where a static broad beam was used as opposed to those on the Cockcroft–Walton where the ion beam was focused and scanned across the target.

Variations in operator and instrument performance are particularly apparent when the data of Fig. 6 and Fig. 7 are compared (e.g. the differing hardness values of unimplanted silicon). The hardness data of Fig. 6 were obtained some four months previous to those of Fig. 7 (the unimplanted control specimens (SU101) and both specimens SI101 and SI108 were remeasured for Fig. 7). However, it is apparent that whatever the absolute values obtained, the trends found in Figs. 6 and 7 are similar, i.e. the 25 gf and 50 gf hardness values decrease with increasing layer thickness and eventually converge towards a common value. It is also important to note that the high-load (large-depth) hardnesses are similar for all specimens as shown in Fig. 11. As expected, the largest errors occur at the lower loads. The largest contribution to this error is probably the finite resolution of the optical system on the Miniload which, with a numerical objective aperture of 0.7, probably limits the accuracy of measuring even an ideal indentation to ~ 0.5 μm [29, 30]. Other errors probably arise from the increasingly plastic nature of the deformation around the indentation at lower loads where pile-up may be significant and can give rise to erroneously large diagonal measurements [27].

Secondly, while it is convenient to talk of a "surface amorphous layer" and to model behaviour in terms of a simple discrete soft layer on a hard substrate, it has to be remembered that the true situation is far more complex than this description suggests. Rather than there being a discrete amorphous–crystalline interface, we would expect a *gradual* structural transition to occur, progressing from amorphous material through highly disordered material and damaged crystal to good crystal over a distance of 0.5 to 1 μm (see Fig. 1). Further, there is also a solute profile from the

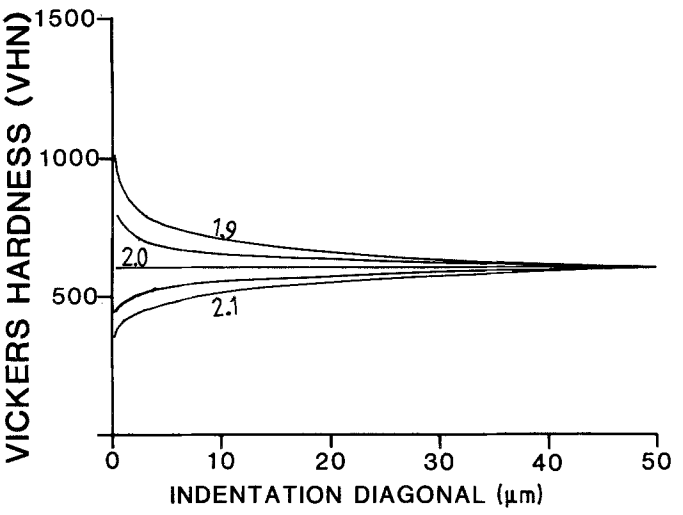

Figure 13 The variation of hardness with changing indentation size for specimens with a 50 μm microhardness of 600 VHN and ISE indices in the range 1.9 to 2.1. The effect of the ISE behaviour only becomes really significant at small indentation sizes (i.e. $\lesssim 4\,\mu m$).

implanted species superimposed on the tail of this damage spectrum as shown in Fig. 1. This would mean that the hardness values derived here as being "characteristic" of the layer should really be taken as an average over the whole range of structures.

The convergence of the 25 gf and 50 gf lines in Figs. 6 and 7, as mentioned previously, indicates that the surface layer has an ISE index of ~ 2. However, consideration of Fig. 13 shows that significant variation of hardness with indentation size (for ISE indices in the range 1.9 to 2.1) occur only below an indentation diagonal of $\sim 4\,\mu m$, which was also our lower limit of measurement. Thus, reliable measurements of hardness at indentation diagonals less than 4 μm would be necessary to provide a better estimate of the ISE index.

Clearly, from the work presented here it is only possible to infer *something* about the nature and properties of the amorphous layer; that is, in the absence of a bulk sample of amorphous silicon, it is impossible to determine more explicitly the hardness and ISE behaviour of the amorphous material.

The accuracy of the amorphous-layer thicknesses measured from RBS spectra is limited by the accuracy of the energy-to-depth calculations. Since constant values of electronic stopping power of the ion by the substrate were used in the calculations of Section 2, no account was taken of the effect on stopping power of the changing composition and structure of the amorphous layer. Thus the resulting depth scale should be taken as probably good to something like 10% [4].

The model proposed for the prediction of the amorphous-layer thickness produced by ion implantation gives fairly good agreement with those values obtained by RBS (with the exceptions of SI106 and SI108). However, it may be seen from Table II and Fig. 8 that, in general, the measured thickness is somewhat greater than that predicted. Thus, if it is assumed that the LSS and WSS models for range and damage distributions are accurate, and that the critical displacement level criterion for amorphization is realistic,* then it may be that an increase in atomic density of the surface during implantation causes an overestimation of the depth of the amorphous layer when interpreting the RBS spectra. Such an increase in atomic density could result from interstitial trapping of the ingoing species, resulting in an effective increase in stopping power of the surface layer. Alternatively, if any surface expansion occurs during implantation (e.g. [31]) then the layer formed will be thicker than predicted. This may also affect the stopping power.

The full range of changes that occur to the target during implantation are as yet unclear. However, it is apparent that some effect results in the rapid growth of the amorphous layer beyond a dose of $\simeq 4 \times 10^{17}\,N_2^+$ ions cm^{-2} (as discussed in Section 4).

*In fact, the thickness of the amorphous layer is fairly insensitive to the exact amorphization criterion used. Consideration of the Gaussian form of the displacement damage curves shows that the thickness $t_a \propto [\ln(\text{dose}) - \ln a]^{1/2}$ where a is the displacement criterion. The curves of Fig. 3 exhibit this behaviour; the amorphization criteria simply determines the intercept of the curves on the dose axis. At doses $\sim 10^{17}$ ions cm^{-2}, the curves would have to be displaced by at least an order of magnitude along the dose axis to account for the discrepancy between the observed and calculated thicknesses.

The model used to predict the hardness behaviour of ion-implanted silicon possessing a surface amorphous layer clearly has many shortcomings. First, it is assumed that there is a definite interface between the soft layer and the substrate and, as has already been discussed, this is not the case. Second, the assumption that the amorphous layer shows no variation of hardness with load (ISE index = 2) may also be valid. However, the experimentally determined value of the ISE index for the layer is ~ 2 and, as has been discussed earlier, small deviations from this value will be insignificant, at least over the range of indentation sizes used here. Hence, it might be expected that the hardness model would not hold for low loads (< 10 gf) where any ISE effect in the surface layer may become important (e.g. due to surface oxide layers, adsorbed layers, chemomechanical effects, etc.).

The geometry assumed for the calculation of $H_{\text{effective}}$ (Fig. 9) may be expected to be valid at large indentation sizes, but at smaller indentation sizes this may not be so. As the indentation becomes increasingly enclosed within the softer layer, the influence of the substrate on the hardness decreases. The rate at which this occurs may be expected to be greater than that predicted by the geometry of Fig. 9, since the softer layer will be able to undergo deformation parallel to the interface (i.e. radial extrusion). The relief of shear stresses by this means results in the surface layer not being rigidly coupled to the substrate, and consequently the volume of substrate, V_1, contributing to the hardness in Equation 7 will be less than that defined in Fig. 9. It would appear that the empirical factor, $V_1/(V_1 + V_2)$, introduced in Equation 9 to some extent takes this into account. However, the mechanics of this situation seems a fruitful area for future theoretical appraisal.

The model is not particularly sensitive to changes in certain variables, in particular the hardness assumed for the softer layer, H_2. Calculation shows that a reduction in the value of H_2 results in a slight shift in position of the peak hardness for a given layer thickness (to the right in Fig. 11) and a steeper decrease in hardness will occur in the region before the point at which the indentation is contained completely within the layer. It is the difference in ISE behaviour between the substrate and the layer that gives rise to the characteristic shape of the computed curves and hence the values of hardness predicted by the model are most sensitive to the hardness–load characteristics of the substrate.

From Figs. 6 and 7 it may be seen that the observed hardness is related to the amorphous layer thickness and that the "critical dose" of Roberts and Page [3] corresponds to a softening due to changes in the amorphous-layer thickness. In this case, the "critical dose" would not have been predicted by the plots of Fig. 3, since the measured amorphous-layer thicknesses deviated significantly from the predicted values (Fig. 8) above the "critical dose" range ($\sim 4 \times 10^{17}$ N_2^+ ions cm^{-2}).

However, the possibility remains that the rapid change in amorphous-layer thickness at doses above the "critical dose" may not completely explain the accompanying marked decrease in surface hardness. Pethica [32] has reported a similar critical dose of $\sim 4 \times 10^{17}$ N^+ cm^{-2} (assumed to be N_2^+ since the implantations were also performed in the Harwell Pimento machine) for surface softening of tungsten carbide, but with the hardness measured using penetration depths much less than the expected mean range (40 to 200 nm). Thus, it may be that the hardness decrease and the rapid increase in thickness of the amorphous layer are themselves *both* caused by some (unspecified) change in the layer structure at the critical dose.

The presence and size of the amorphous layer is obviously the prime factor in determining the hardness behaviour of the ion-implanted material tested here. However, the possibility of softening by interaction between the implanted atoms and moving dislocations is not disproved by this study, but merely shown to be insignificant (if indeed it exists). It is interesting to note that no significant difference in hardness was found between silicon wafers with differing bulk dopants, either in this study or by other workers (e.g. [33, 34]), though changes in dislocation etch pit rosette lengths around hardness indentation have been reported to be dopant sensitive [35].

8. Conclusions

The work presented here gives an important insight into the way in which surface mechanical properties, specifically hardness, may be influenced by ion-implantation-induced structural changes in silicon. Other covalently bonded materials, e.g. SiC and diamond, might be expected to behave in a similar manner.

It has been shown that a surface amorphous layer may be produced by implantation with a

range of group III, IV and V elements and that the thickness of the layer produced is a function of dose, energy and ion mass as expected.

The thickness of the amorphous layer produced may be modelled with good correlation between the predicted and the experimentally determined layer thicknesses at doses of $< 5 \times 10^{17}$ ions cm^{-2} for the ion species and energies used here. For nitrogen ions, when a dose of around 4×10^{17} N_2^+ cm^{-2} is exceeded, it is found that the model no longer holds. The model used to predict amorphous-layer thickness show how the position of the layer (e.g. surface or sub-surface is expected to vary with dose). Further, the criterion of 0.1 DPA for amorphization seems to give reasonable agreement with the observed behaviour.

The hardness behaviour of the ion-implanted silicon reveals that the amorphous layer is softer than the substrate (the estimated hardness of the layer is 400 to 700 VHN) and exhibits little or no indentation size effect (ISE).

The "critical dose" for softening reported by Roberts and Page [3] has been shown to correspond to the dose range over which the amorphous layer (unexpectedly) grows sufficiently thick to enable the indentation size used for testing ($\sim 10\,\mu m$ diagonal) to lie substantially within the layer.

The attempt to model the low-load (< 1 kgf) hardness behaviour of a thin compliant layer on a hard substrate has at least established the need to consider the ISE behaviour of both layer and substrate as well as their relative hardnesses. Though the model seems capable of predicting the correct trends observed in hardness–indentation-size behaviour of the composite structure, the absolute values of hardness predicted (e.g. the curves in Fig. 11) depend critically on both the hardness and the ISE behaviour of silicon but less so on the behaviour of the layer.

In conclusion, it has been established that the low-load hardness behaviour of ion-implanted silicon is intimately related to the extent of the structural changes produced by high-dose ion implantation. Further, the effects observed here depend solely on implantation producing a near-surface amorphous region rather than on the identity of the ion species introduced, though this may be important in other systems (e.g. [15]).

Acknowledgements

The authors are indebted to Professor R. W. K. Honeycombe for provision of laboratory facilities, to the University of Cambridge Computing Service for provision of computing facilities, and to Dr G. Dearnaley and Dr N. Eyre for provision of, and technical assistance with, both the implantations and the RBS analysis. Dr E. Yoffe is thanked for helpful discussions. PJB wishes to acknowledge the SERC and AERE Harwell for the provision of a CASE Award. We are also grateful to Mr P. J. C. Mathis (Texas Instruments Ltd (UK)) for the provision of silicon samples.

References

1. G. DEARNALEY, *Nucl. Inst. Methods* **189** (1980) 117.
2. *Idem, Trans. Inst. Met. Finish.* **56** (1978) 25.
3. S. G. ROBERTS and T. F. PAGE, "Ion Implantation into Metals", edited by V. Ashworth, W. A. Grant and R. P. M. Proctor (Pergamon, Oxford, 1982).
4. G. CARTER and W. A. GRANT, "Ion Implantation of Semiconductors" (Edward Arnold, London, (1976).
5. J. LINDHARD, M. SCHARFF and H. E. SCHIØTT, *Matt. Fys. Med. Kgl. Dansk. Vid. Selsk.* **35** (1966) No. 9.
6. B. J. SMITH, as tabulated in ref. 11.
7. K. B. WINTERBON, P. SIGMUND and J. B. SANDERS, *Matt. Fys. Med. Kgl. Dansk. Vid. Selsk.* **37** (1970) No. 14.
8. G. H. KINCHIN and R. S. PEASE, *Rep. Prog. Phys.* **18** (1955) 1.
9. G. CARTER and J. S. COLLIGON, "Ion Bombardment of Solids" (Heinemann Educational, London, 1968).
10. B. T. KELLY, "Irradiation Damage to Solids" (Pergamon, Oxford, 1966).
11. G. DEARNALEY, J. H. FREEMAN, R. S. NELSON and J. STEPHEN, "Ion Implantation" (North-Holland, Amsterdam, 1973).
12. L. A. CRISTEL, J. F. GIBBONS and T. W. SIGMON, *J. Appl. Phys.* **52** (1981) 7143.
13. J. F. ZIEGLER, "He; Stopping Powers and Ranges for all Elements" (Pergamon, Oxford, 1977).
14. D. C. JOY, D. E. NEWBURY and D. L. DAVIDSON, *J. Appl. Phys.* **53** (1982) R81.
15. P. J. BURNETT, unpublished work, 1983.
16. S. M. DAVIDSON and G. R. BOOKER, *Rad. Eff.* **6** (1970) 33.
17. G. W. LEWIS, G. KIRIAKIDES, G. CARTER and M. J. NOBES, *Surf. Interface Anal.* **4** (1982) 141.
18. G. R. SAWYER, P. M. SARGENT and T. F. PAGE, *J. Mater. Sci.* **15** (1980) 1001.
19. P. M. SARGENT and T. F. PAGE, *Proc. Brit. Ceram. Soc.* **26** (1978) 209.
20. P. E. DONOVAN and W. M. STOBBS, *Acta Metall.* **29** (1981) 1419.
21. P. M. SARGENT and P. E. DONOVAN, *Scripta Metall.* **16** (1982) 1207.
22. H. BÜCKLE, "The Science of Microhardness Testing and its Research Applications", edited by J. H.

Westbrook and H. Conrad (American Society for Metals, Ohio, 1973) p. 453.
23. M. J. MATTHEWSON, *J. Mech. Phys. Solids* **29** (1981) 89.
24. P. M. SARGENT, PhD thesis, University of Cambridge (1979).
25. K. L. JOHNSON, *J. Mech. Phys. Solids* **18** (1970) 115.
26. C. J. STUDMAN, M. A. MOORE and S. E. JONES, *J. Phys. D.* **10** (1977) 949.
27. P. M. SARGENT and T. F. PAGE, *Scripta Metall.* **25** (1981) 245.
28. "Handbook of Chemistry and Physics", edited by R. C. Weast, (CRC Press, Ohio, 1977) p. B218, and p. F80.
29. I. C. LEIGH and G. N. PEGGS, NPL Report MOM 47 (1980).
30. H. BÜCKLE, *Z. Metallkde* **45** (1954) 623.
31. K. WITTMAACK and G. STAUDENMAIER, *J. Nucl. Mater.* **94** (1980) 581.
32. J. B. PETHICA, "Ion-Implantation into Metals", edited by V. Ashworth, W. A. Grant and R. P. M. Proctor (Pergamon, Oxford, 1982) p. 147.
33. M. G. S. NAYLOR and T. F. PAGE, annual technical report contract No. DAERO-78-G-010, European Research Office, United States Army, London, 1980.
34. M. G. S. NAYLOR, PhD thesis, University of Cambridge (1982).
35. S. G. ROBERTS, P. PIROUZ and P. B. HIRSCH, *J. Phys. (Colloque)*, (1983) (in press).

Received 15 June
and accepted 28 June 1983